Acidic Properties of H−β Zeolite As Probed by Bases with Proton Affinity in the 118−204 kcal mol−1 Range: A FTIR Investigation

ARTICLE *in* THE JOURNAL OF PHYSICAL CHEMISTRY B · JUNE 1997

Impact Factor: 3.3 · DOI: 10.1021/jp970649z

5 AUTHORS, INCLUDING:

Carlo Lamberti
Università degli Studi di Torino
379 PUBLICATIONS **13,129** CITATIONS

SEE PROFILE

A. Zecchina
Università degli Studi di Torino
560 PUBLICATIONS **19,938** CITATIONS

SEE PROFILE

Acidic Properties of H−β Zeolite As Probed by Bases with Proton Affinity in the 118−204 kcal mol^{-1} Range: A FTIR Investigation

C. Pazé, S. Bordiga, C. Lamberti, M. Salvalaggio, and A. Zecchina*

Dipartimento di Chimica Inorganica, Chimica Fisica e Chimica dei Materiali, Università di Torino, Via P. Giuria 7, I-10125 Torino, Italy

G. Bellussi

ENI RICERCHE, Via F. Maritano 26, I-20097 S. Donato, Milan, Italy

Received: February 21, 1997[⊗]

The interaction of Brønsted sites of H−β (AH) with bases B with proton affinity (PA) ranging in the 118 (N_2) to 204 (NH_3) kcal mol^{-1} interval leads to the formation of 1:1 adducts. The vibrational manifestations of these adducts change considerably as a function of the proton potential. In 1:1 neutral adducts characterized by weak-medium hydrogen bonds, the shift of the ν(AH) mode ($\Delta\bar{\nu}$) is proportional to the shift caused by the same bases on the Si−OH (weak) Brønsted acid used as a standard. As far as the 1:1 adducts formed with ethers and tetrahydrofuran (THF; PA = 196 kcal mol^{-1}), the situation is more complex owing to high ionicity acquired by the hydrogen bond. When stronger bases are used (pyridine, Py), the true proton transfer is observed. The ν(AH···B) modes of the medium-strong 1:1 adducts are modulated by Fermi resonances with 2δ and 2γ overtones and with internal modes of A and B moieties. A general review of the phenomenon is given. Also the spectra of the ionic 1:1 adducts formed with Py and NH_3 are modulated by complex Fermi resonance effects. The situation occurring at higher dosages of B is also examined: it is concluded that in the presence of an excess of H_2O (and CH_3OH) the originally formed neutral 1:1 adducts are transformed into protonated clusters.

1. Introduction

The protonic form of the zeolite β is an active catalyst in a variety of reactions, like hydrocarbon cracking,[1] alkylation of aromatic hydrocarbons,[2−4] alkane hydroisomerization,[5] and conversions of methanol and other oxygen compounds.[6] It has catalytic activity also in the alkali form (alkylation of aniline)[7] and when substituted by metals like Ti (oxidations by hydrogen peroxide)[8] and Ga (Knoevenagel condensation)[9] or by elements like Ge[9] and B (*m*-xylene isomerization).[10] Finally, β zeolite supporting Pt is active in re-forming and aromatization of *n*-hexane.[11] If lots of efforts have been and are made in the direction of the study of reactivity, not the same quantity of studies, on the contrary, has been made to understand the fundamental properties of the protonic form of the zeolite β, such as the acid strength of Brønsted and Lewis acid sites, and the influence of the particular framework structure (dimensions of the channels, presence of crystal defects, positions of protons). The measurement of the acid strength of Brønsted and Lewis sites in a zeolitic framework (and in general in a solid) does not have a single experimental approach, and titration methods,[12−14] calorimetric measurements,[15,16] and spectroscopic techniques have been used to this purpose. In particular, Parrillo et al.[15,16] have shown that (i) as far as H−ZSM-5 is concerned, the adsorption enthalpy of amines (proton affinity (PA) in the 205−224 kcal mol^{-1} interval) is linearly correlated with the proton affinities of the same molecules in the gas phase; (ii) the adsorption enthalpies of NH_3 on H−ZSM-5, H−ZSM-12, and H−Y are practically identical. Among the spectroscopic techniques, IR and solid state NMR have been used to discriminate among acid sites (i.e., Lewis and Brønsted) of different strength. The classical IR spectroscopic way to study the acidity of Brønsted sites in zeolites is to measure the perturbation of the associated vibrational modes upon interaction with bases. The method is based on the experimental observation that the formation of AH···B adducts between a Brønsted acid AH and a base B via the acid−base type reaction

$$\mathrm{AH} + \mathrm{B} \rightleftharpoons \mathrm{AH}\cdots\mathrm{B}$$

is accompanied by a downward shift of the ν(AH) ($\Delta\bar{\nu}$), which is proportional to the reaction enthalpy. This effect, initially documented for homogeneous systems (solutions),[17] is also verified for the heterogeneous systems like zeolites[18,19] and oxides.[20,21]

Since a complete set of spectroscopic results is not available for H−β except for a few basic molecules (H_2O,[22] benzene,[22] pyridine (Py),[22−25] hexane,[22] NH_3[25,26]) and in limited spectral ranges, we think that more data and results should be added. We present here an IR spectroscopic study of the interaction of the OH Brønsted sites of H−β (Si/Al = 12.5) with a great variety of molecules of different gas phase proton affinity and dimensions, such as N_2 (PA = 118.2 kcal mol^{-1}), CO (PA = 141.9 kcal mol^{-1}), C_2H_4 (PA = 162.6 kcal mol^{-1}), C_3H_6 (PA = 179.5 kcal mol^{-1}), H_2O (PA = 166.5 kcal mol^{-1}), CH_3CN (PA = 188.6 kcal mol^{-1}), CH_3OH (PA = 181.9 kcal mol^{-1}), $(CH_3)_2O$ (PA = 192.1 kcal mol^{-1}), tetrahydrofuran (THF) (PA = 196 kcal mol^{-1}), and Py (PA = 204 kcal mol^{-1}). In this paper the shift $\Delta\bar{\nu}$ will be measured for each base B and compared with that obtained on other acidic zeolites and other acidic systems. Owing to the complexity of the IR spectra of NH_4^+ (associated with the presence of four NH groups which can variably interact via hydrogen bonding with the zeolite skeleton), a detailed discussion of the NH_3/H−β interaction is

* Author to whom correspondence should be addressed. Tel, +3911 6707537; fax, +3911 6707855; e-mail (Internet) ZECCHINA@silver.CH.UNITO.IT.

⊗ Abstract published in *Advance ACS Abstracts,* May 1, 1997.

S1089-5647(97)00649-4 CCC: $14.00

postponed to a separate contribution where also the NH_3/H−ZSM-5, NH_3/H−mordenite (H−MORD), NH_3/H-SAPO, and NH_3/H−Y systems will be considered.[27] Due to the great increase of basicity on passing from the first to the last probe molecule B, the spectroscopic effects caused on the vibrational modes of the acidic sites upon formation of the acid−base adducts are expected to change gradually and to become very large and complex for the adducts formed with the strongest bases. In order to shorten and to facilitate the description and the comprehension of the experimental spectra, a summary of the main spectroscopic characteristics expected for such series of hydrogen-bonded systems is briefly outlined. This summary, based on the well-established and fully understood experimental features of the H-bonded AH···B in homogeneous systems, is used as starting base for understanding the intra-zeolitic H-bond interactions.

2. Experimental Section

Well-crystallized zeolite β samples including template triethylamine (TEA), prepared following the procedure illustrated in ref 28, were supplied by ENIRICERCHE Laboratories of S. Donato Milanese (Milan, Italy). The β samples used in these experiments are characterized by an average particle size of 1−2 μm and a surface specific area of 750 $m^2\ g^{-1}$. The elementary chemical analysis indicates that the Si/Al ratio is 12.5 and that the amount of alkali-metal ions is less than 100 ppm. H−β samples have been obtained from the β samples including the template by thermal treatment under high vacuum, following a procedure involving a gradual temperature rise from 300 to 673 K at a 200 K/h speed. After this treatment the sample was kept at 673 K for 1 h, and the template residues were burned off in the presence of O_2 (13 kPa) at 723 K, for 45 min. The zeolite samples were in the form of self-supporting wafers, and the IR spectroscopic measurements have been effected on a Bruker 66 instrument equipped with a MCT cryogenic detector, performing at 2 cm^{-1} resolution. CO, N_2, C_2H_4, and C_3H_6 where of high-purity grade from Matheson and were used without further purification. Distilled H_2O and CH_3CN, CH_3-OH, $(CH_3)_2O$, THF, and Py from Aldrich have been further purified by repeated freeze−pump−thaw cycles. All of the gases and vapors were dosed from a vacuum manifold permanently attached to the IR cells. The dosed amounts corresponding to each IR spectrum were estimated by measuring the pressure drop when known doses of the gases and vapors were allowed to contact the sample. The obtained figures can be considered accurate only for doses of B lower or equal to those needed to give stoichiometric B/Brønsted (1:1) adducts (because they correspond to the maximum drop of the pressure). The amounts of adsorbed H_2O, CH_3CN, CH_3OH, $(CH_3)_2O$, and THF were also determined gravimetrically in a parallel experiment by means of a CAHN System 113 microbalance. The attainment of the 1:1 Brønsted groups/base stoichiometry has been also confirmed by the simultaneous complete disappearance of the IR peak of the unperturbed Brønsted groups. In conclusions, we think that the attainment of 1:1 stoichiometry has been estimated with an error not greater than 10%. The IR measurements involving N_2, CO, and propene were effected in special low-temperatures cells (N_2 and CO at 100 ± 10 K and C_3H_6 at 180 ± 10 K), while all of the other measurements have been conducted at room temperature. As far as CO, N_2, and propene are concerned, the intensities of the IR bands due to hydrogen bonded species were not appreciably time dependent: this indicates that equilibrium conditions were quickly reached in all cases. As for the other bases, the spectra were taken after about 1 min, which is a time interval sufficient to ensure the attainment of time independent spectra.

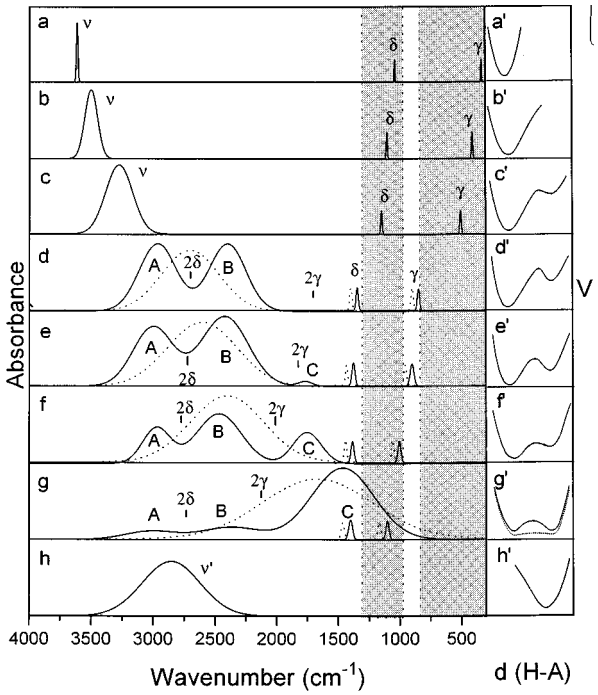

Figure 1. (a−h) Qualitative representation of the IR spectroscopic features of weak, medium, and strong A−H···B or A^-···$H-B^+$ H-bonded complexes. The half-width of the bending modes is assumed somewhat arbitrarily to slightly increase upon increasing the hydrogen bond strength. The gray areas correspond to regions obscured by the skeletal modes of the zeolite framework. (a′−h′) Schematic representation of the correlated evolution of the proton potential as function of the A−H distance in A−H···B or A^-···$H-B^+$, following ref 39. The separation barrier in e′−f′ can be very low, and a potential curve characterized by an asymmetric single flat minimum could be used in place.

As for the H−ZSM-5, H−MORD, and H−Y samples cited in Table 1 and in Figure 3, they have Si/Al ratios respectively of 14, 5, and 3, and they have been studied by the authors in refs 29−35. While the H−ZSM-5 sample was constituted by nanosized microcrystals (external surface area ca. 50 $m^2\ g^{-1}$), the external surface area of H−MORD and H−Y was 1 order of magnitude lower. H−Y, H−ZSM-5, and H−MORD were obtained by controlled thermal decomposition (673 K) of the ammonium precursor forms; zeolite Y was a commercial Union Carbide sample, while ZSM-5 and MORD were supplied by ENICHEM laboratories.

3. Results and Discussion

3.1. Basic IR Spectroscopy of AH···B and AH^+···B^- Systems: A Short Review. The spectroscopy of the homogeneous AH···B systems comprising an acid AH and a base B can be outlined by briefly describing five representative situations: (i) AH isolated, (ii) AH interacting with B through a weak H-bond, (iii) AH interacting with B through a H-bond of medium-strong strength, (iv) AH interacting with B through a strong H-bond, and (v) A^-···$^+$HB hydrogen bonded ionic pairs, corresponding to the proton transfer.

(i) AH Unperturbed. If A is not a single atom, the unperturbed AH oscillator is characterized by three vibrational modes, the stretching ν and the bending modes δ and γ (in and out of the plane) (Figure 1a, left hand side). The proton potential of the unperturbed AH is that typical of an anharmonic oscillator, the shape of the function being that of a curve with a single minimum (Figure 1a′, right hand side).

(ii) AH Interacting with B through a Weak H-Bond. In consequence of the interaction, the ν(AH) stretching undergoes

a negative shift ($\Delta\bar{\nu}$) comprised in the 0−400 cm^{-1} interval and a proportional increase of the integrated intensity (ΔI) and of the full width at half-maximum (FWHM; ΔFWHM). At the same time, the bending modes δ and γ shift to higher frequencies. This is schematically represented in Figure 1b,c (full line spectra). An empirical correlation exists between $\Delta\bar{\nu}$ and FWHM, as FWHM $\cong 0.75\Delta\bar{\nu}$.[17] $\Delta\bar{\nu}$, ΔI, and ΔFWHM are proportional to the enthalpy of formation of the H-bond.[17] The increase of the integrated intensity and of FWHM is due to anharmonic coupling between the ν mode and the low-frequency external mode ν(A···B) (in turn coupled with the thermal bath fluctuations[36]). Because of this anharmonic coupling, the ν(AH···B) mode can be better described as a continuum. Upon formation of a weak hydrogen bond, the proton potential becomes more anharmonic and the equilibrium AH distance increases (Figure 1b,c).

(iii) AH Interacting with B through a H-Bond of Medium-Strong Strength. Upon formation of AH···B adducts characterized by hydrogen bonds of medium strength, $\Delta\bar{\nu}$ gradually increases up to 1000 cm^{-1}, with parallel increase of the FWHM and I (Figure 1d, dotted curve). However, the spectroscopy of H-bonded systems of medium strength is not so simple as illustrated by the dotted curves, because the shape of the bands is deeply modified by Fermi resonance effects with 2δ and 2γ overtones (Figure 1d−f). As is well-known, Fermi resonance occurs between two very close vibrational levels of proper symmetry: as a consequence the two original modes mix together and originate two different bands, each of them being a mixture of the original modes.[37] According to a simplified approach,[38] the Fermi resonance between the ν(AH···B) and the 2δ and 2γ modes of (AH···B) in medium strength hydrogen-bonded systems modifies the profile of the ν mode with the appearance of up to three components (A−C). The simplest case is verified when the maximum of the band of the ν(AH···B) coincides with the 2δ (Figure 1d) and when the 2γ frequency is still far from the maximum of the ν(AH···B) band. In this case the ν(AH···B) is splitted into two bands of equal intensity (A, B), while the C band appears on the extreme low-frequency flank with very low or negligible intensity. The corresponding potential shape is represented in Figure 1d′.

For medium-strong hydrogen bonds, $\Delta\bar{\nu}$(AH···B) increases and both the 2δ and 2γ frequencies become internal to the further broadened ν(AH···B) continuum; three bands are consequently generated, named A, B, and C, whose relative intensity changes gradually from $I_A \cong I_B \gg I_C$ to $I_A < I_B \cong I_C$ with the increase of the strength of the hydrogen bond (from medium to strong) and the decrease of the AB distance in the AH···B complex.

Bands of this type are well-known in literature and are usually considered to correspond to proton potential functions consisting of an asymmetric double minimum, with a gap of energy between the two minima, decreasing as the strength of the H-bond increases (Figure 1d′−f′).[39] The present description is only qualitative, since the real shape of the potential for hydrogen bonds corresponding to shifts $\Delta\bar{\nu} = 1000$ cm^{-1} is not really well-established. Parallel to the hydrogen bond strength increase, the tunneling probability increases too, and a clear localization of the proton becomes increasingly difficult, due to its fast fluctuation among the two limit structures under the effect of external perturbations: the system consequently evolves progressively toward more polar forms.

(iv) AH Interacting with B through a Strong H-Bond. For very strong H-bonds the interaction energy between AH and B reaches its maximum value, and correspondingly $\Delta\bar{\nu}$ also reaches its maximum ($\cong$2000−2500 cm^{-1}), while the AB distance reaches its minimum (Figure 1g,g′). Following Böhner and Zundel,[39] under these circumstances the potential function of the proton is characterized by a symmetric double minimum curve, with a very low gap of energy between the two minima, or by a single broad and flat minimum (Figure 1g′). In both cases the AH···B and $A^-\cdots{}^+HB$ structures have comparable weight in the description of the system.[39] Under these conditions, the nearly complete disappearance of the A and B components is usually observed, and only the C component remains as the dominating feature. This C band (often called "D") is a very intense, broad band, extending toward low frequencies (Figure 1g). This absorption is generally modulated by a large variety of narrow Evans windows caused by direct resonant interaction with the δ (and perhaps the γ) mode and with the internal modes of the A and B moieties. In consequence of this fact, the IR spectrum of strongly hydrogen-bonded complexes is very complex, and its detailed assignment is often not well-known.

(v) Formation of $A^-\cdots{}^+HB$ Adducts. When the proton affinity of B approaches 200 kcal mol^{-1} (NH_3, Py), the H-bond interaction between AH and B can be followed by a proton transfer reaction leading to the formation of the anion A^- and the protonated $^+$HB hydrogen bonded pair. The probability that protonation can really occur does not depend only on the strength of the H-bond (and so, on the PA of the reactants), but also on the stabilization of the ionic pairs: this stabilization is due, in homogeneous conditions, to solvent effects and, in heterogeneous conditions, to the interaction with the surfaces.[15,16] Remembering the elementary concept that the stronger is the base B and the weaker is the hydrogen bond in the ($A^-\cdots{}^+HB$) pair, the IR spectroscopy of the pair becomes similar again to that of the hydrogen-bonded systems of medium strength (Figure 1h). The frequency of the $\nu(BH^+\cdots{}^-A)$ band increases while the $\Delta\bar{\nu}$, FWHM, and I decrease. In Figure 1h, no attempt is made to localize the δ and γ modes, since they are heavily mixed with internal modes of BH^+ (ring modes in the case of PyH^+).[40]

3.2. Structure of the β Zeolite and the IR Spectrum of the Virgin Sample. Zeolite β is a 12-membered ring zeolite having a three-dimensional pore system of channels, two linear and one tortuous. It can be regarded as a highly intergrown hybrid of two distinct but related structures, named polimorphs A and B, both deriving from different arrangements of stacking sequences of the same chiral structural building block.[41−43] Polimorph A has a tetragonal[43] cell, and it is equipped with a pore stacking "abab" type; polimorph B is described by a triclinic[41] or monoclinic[43] cell and has an "abc" pore stacking sequence. Since the X-ray powder diffraction pattern consists of a combination of broad and sharp reflections,[43,44] it is considered that zeolite β has an extensively faulted structure. In fact, it has been calculated with lattice energy minimization procedures[45] that there is not a particular energetic preference for polimorph A or polimorph B, so that zeolite β generally contains the two phases in roughly equal proportion and a high degree of stacking disorder is present. The stacking disorder phenomena have the consequence of generating unsatisfied linkages (for example in the regions of the connection of the two polimorphs), so the presence of a high concentration of hydroxyl groups in zeolite β has been suggested.

The IR spectrum of β zeolite, after outgassing at 673 K in vacuo, shows three types of bands at 3749, 3614, and 3000−3500 cm^{-1} (very broad) (Figure 2, top spectrum). The sharp peak at 3749 cm^{-1} is due to the OH vibration of free silanols SiOH (i.e. silanols not interacting through hydrogen bonds, because they are isolated or in terminal positions); the band at

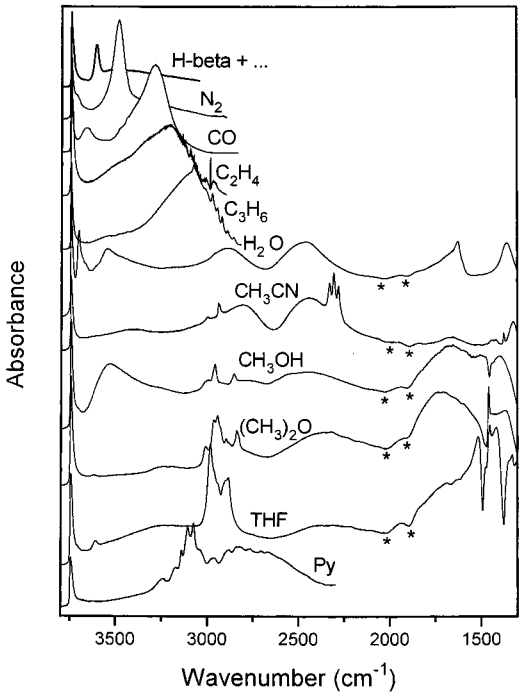

Figure 2. Background subtracted IR spectra of H−β/B 1:1 adducts (B = N_2, CO, C_2H_4, C_3H_6, H_2O, CH_3CN, CH_3OH, $(CH_3)_2O$, THF, Py). The asterisks indicate the "false" bands due to the effects of bases adsorption on the zeolite skeletal modes as discussed in ref 29.

3614 cm^{-1} is the OH stretch of strongly acidic bridging hydroxyls. As for the broad band in the 3000−3500 cm^{-1} interval, it has been attributed either to SiOH groups in framework defect sites (nests) interacting through hydrogen bonds[46] or to distorted[47] bridged hydroxyl acid groups interacting with oxygen atoms of the framework.[22] Due to the accurate thermal treatment adopted in this work to eliminate the templating agent, no bands at 3660−3680 and at 3782 cm^{-1} (already reported by Kiricsi et al.[22] and attributed to low-acidity OH groups bonded to extralattice aluminum[31]) are observed: this means that in our sample nearly all aluminum is in frame (tetracoordinated) positions. If the templating agent is burned in air following the usual procedure, a relevant fraction of aluminum goes into extraframework positions, and an absorption at 3660−3680 cm^{-1} is consequently present in the background due to hydroxyl groups in extralattice aluminum.

3.3. IR Spectra of 1:1 Adducts Obtained by Interaction with Bases of Proton Affinity Ranging in the 118−204 kcal mol^{-1} Range: General Features. The effect of the interaction with molecules (B) of different gas phase PA on the strong Brønsted sites (ν(OH) at 3614 cm^{-1}) is shown in Figure 2. The reported spectra refer to a dosage corresponding roughly to the formation of (OH···B) 1:1 adducts. Under these conditions almost all of the strong Brønsted sites have reacted with B, while isolated silanols (3749 cm^{-1}) are left nearly completely unperturbed.

Without detailing too much for reasons of conciseness, it is clear that a close analogy exists between Figure 1 and Figure 2. This observation allows us to reach the following conclusions:

(i) The resonant origin of the ABC triad observed on acidic zeolites and originally advanced by Pelmenschikov et al.[48,49] is totally confirmed.

(ii) The strength of the hydrogen bond progressively grows as the proton affinity increases, and reaches its maximum when the value of the gas phase PA is about 196 kcal mol^{-1} (THF) ($I_C \gg I_B > I_A$). The last situation corresponds to a proton potential with a symmetric double minimum having a very low gap, or even with a single broad flat minimum.

(iii) A complete proton transfer takes place with the formation of $A^-\cdots{}^+HB$ only when PA is larger than 200 kcal mol^{-1} (Py).

TABLE 1: Spectroscopic Data of the Modes of Brønsted Sites/B 1:1 Adducts (cm^{-1})[a]

	Al(OH)Si						SiOH
B	$\bar{\nu}_A$	$\bar{\nu}_B$	$\bar{\nu}_C$	$\bar{\nu}(\delta)$	$\bar{\nu}(\gamma)$	$\Delta\bar{\nu}$	$\Delta\bar{\nu}$
N_2						126	37
CO						319	90
C_2H_2						350	124
C_2H_4						410	126
C_3H_6						514	165
H_2O	2820	2450	1700	1352	880	914	300
CH_3CN	2850	2470	1660	1320	875	975	330
CH_3OH	2880*	2460	1550*			1460	410
CH_3CH_2OH	2880*	2425	1550*			1720	420
$(CH_3)_2O$	2850*	2370	1600*			1670	430
$(CH_3CH_2)_2O$	2870*	2320	1400*			1815	460
THF	2900*	2320	1400*			1865	480

[a] Frequency values labeled with an asterisk are affected by ±50 cm^{-1} uncertainty. Shifts $\Delta\bar{\nu}$ of the ν(OH) mode of strong Brønsted sites have been calculated following refs 18 and 38.

According to the approach of Odinikov and Jogansen[38] and of Kubelková et al.,[18] it is possible to calculate, from the intensities and the frequencies of the A, B, and C bands, the position of the barycenter of the ν(OH) mode in the absence of Fermi resonances effects. Because of the difficulties associated with the estimation of the intensity and the frequencies of the ABC components, such frequencies must be considered to have a precision of ±50 cm^{-1}. However, for shifts $\Delta\bar{\nu}$ ranging between 1000 and 2000 cm^{-1}, a total uncertainty of 100 cm^{-1} is tolerable. In Table 1 the shifts $\Delta\bar{\nu}$ caused by the interaction with bases of increasing gas phase PA are reported.

The spectra of N_2, CO, H_2O, and THF will be accurately described later, examining also situations corresponding to acid site/base ratios greater than 1.

The spectra of C_2H_4 and of C_3H_6 have been taken after short contact times in order to avoid oligomerization (that occludes the pores and complicates the interpretation of the spectra), using a procedure already described.[50,51] The spectrum of CH_3CN at room temperature shows a triad of bands A (2807 cm^{-1}), B (2447 cm^{-1}), and C (1659 cm^{-1}), and it is similar to that already studied for CH_3CN interacting with H−MORD and H−ZSM-5. The band at 1320 cm^{-1} is the δ_{OH} mode shifted by interaction with the strong Brønsted acid site; the corresponding γ_{OH} mode is at 875 cm^{-1} (spectra not reported for sake of brevity). For more details the reader is referred to ref 29.

The C band in the spectra of CH_3OH, $(CH_3)_2O$, and THF is modulated in a very spectacular and characteristic way by Fermi resonances with the methyl bending modes of appropriate symmetry. In particular the spectra of CH_3OH and of $(CH_3)_2O$ are very similar to those observed in H−ZSM-5 and in H−MORD,[30] and the reader is referred to them for a detailed assignment. As found before on these systems, a localization of the δ band is nearly impossible because it is overshadowed by the strong C component. Moreover, direct resonance effects are not excluded.

The spectrum of Py has been already fully discussed in ref 40. It is worth recalling how the broad band of $\nu(NH^+)$ in the adduct $PyH^+\cdots Z^-$ (Z^- = zeolate anion) is modulated by a set of Fermi resonances associated with the ring modes.

The spectrum of NH_3 is not reported in Figure 2. We shall discuss this spectrum in a separate contribution.[27] For the time being let us anticipate that the spectrum clearly indicates the formation of $NH_4^+\cdots Z^-$ species and that although complicated

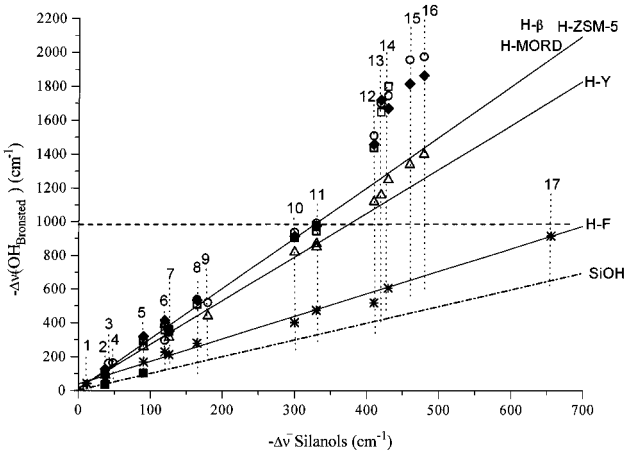

Figure 3. Plot of the shifts ($\Delta\bar{\nu}$) of the $\nu(OH)_{Brønsted}$ frequencies in 1:1 hydrogen bonded complexes of H−β, HF, H−Y, H−ZSM-5, and H−MORD, with different basis *vs* the shifts ($\Delta\bar{\nu}$) of SiOH groups in 1:1 hydrogen complexes with the same bases. Vertical dotted lines labeled with numbers correspond to the following: (1) O_2; (2) N_2; (3) N_2O; (4) CO_2; (5) CO; (6) C_4H_4S, C_2H_2; (7) C_2H_4, C_6H_6, C_4H_6; (8) C_4H_4O, C_3H_6; (9) HC_2CH_3; (10) H_2O; (11) CH_3CN, CH_3CO; (12) CH_3-OH; (13) CH_3CH_2OH; (14) $(CH_3)_2O$; (15) $(CH_3CH_2)_2O$; (16) THF; (17) NH_3. ♦ represents the experimental data of H−β reported in Table 1; ■ represents the experimental data of H−β/H_2O in interaction with N_2 and CO; ∗ represents the experimental data of HF;[59a−f] △ represents the experimental data of H−Y (see ref 30 and references therein); ○ represents the experimental data of H−ZSM-5 (see ref 30 and references therein); □ represents the experimental data of H−MORD (see ref 30 and references therein). For each zeolite, the straight lines approximate the experimental points only for $\Delta\bar{\nu}_{Brønsted} \leq 1000$ cm^{-1}.[30] The dotted-broken straight line corresponds to the $\Delta\bar{\nu}_{SiOH}$ vs $\Delta\bar{\nu}_{SiOH}$ plot.

by the presence of four NH groups, it is basically similar to that of the $Z^-\cdots{}^+HPy$ adducts (because the $\bar{\nu}(NH^+\cdots Z^-)$ bands fall in the same interval).

3.4. $\Delta\bar{\nu}(OH)_{Brønsted}/\Delta\bar{\nu}(OH)_{silanols}$ Correlation. Once the strong Brønsted groups have been fully consumed because of the formation of the OH···B adducts, further dosage of B leads to the progressive consumption of the silanols (which are Brønsted sites of weaker acidity) and also to the formation of liquid-like species in the channels. For the sake of brevity the initial formation of silanol adducts will be documented in detail only for N_2, CO, H_2O, and THF (vide infra section 3.5). From previous considerations, it is evident that, by investigating the whole spectroscopic isotherms, we have the opportunity to verify the effect of the same base on two Brønsted sites of different strength present in the *same solid* (and characterized by a very similar environment). This is true not only for the simplest bases like N_2 and CO but also for other bases like C_2H_2, C_2H_4, C_3H_6, H_2O, CH_3CN, CH_3OH, CH_3CH_2OH, $(CH_3)_2O$, $(CH_3CH_2)_2O$, and THF. The shifts $\Delta\bar{\nu}$ obtained by interaction of these bases with silanols are reported in Table 1 and are identical to those found on silica and on silicalite.[31,34,50−56] The $\Delta\bar{\nu}$ values of the stretching band of silanols and of strong Brønsted groups are plotted in Figure 3. In the same figure the $\Delta\bar{\nu}$ obtained for H−ZSM-5, H−MORD, H−Y,[30] and HF[58] are also reported for the sake of comparison. This kind of plot is suggested by the well-known fact that, in solution,[57,58] it is possible to study the properties of an acid solute X−H, by directly comparing the $\Delta\bar{\nu}$ frequency shift of ν(X−H) caused by the formation of the 1:1 XH···B adduct with that caused by the same base on a second different solute X′−H (for instance, pyrrole used as a standard). This has been verified in a variety of solvents.[57,58] For each solute and for hydrogen bonds of weak-medium strength, linear relationships are constantly observed, and the relative slopes of the straight lines obtained for different X−H systems have been correlated with the pK_a values of the solutes in aqueous solutions. From this figure it is clearly emerging that, as fully discussed in ref 30, a linear relationship exists also between the $\Delta\bar{\nu}$ shifts of the stretching mode of the surface strong Brønsted sites of H−β, H−ZSM-5, H−MORD, and H−Y (caused by interaction with a wide range of basic molecules of increasing gas phase PA) and the $\Delta\bar{\nu}$ of silanols (used as standards)[30] and that the slope of the straight line is a characteristic parameter of each zeolite. The universal validity of this correlation is proved also by the fact that the shifts $\Delta\bar{\nu}$ of the silanols stretching correlate linearly even with the shifts obtained for HF interacting with the same bases in an argon matrix,[59] which is not obvious because of the different "solvents" (zeolite framework and argon). It is also evident that, as already discussed in ref 30, the linear correlation illustrated in Figure 3 holds only for $\Delta\bar{\nu}$ of strong Brønsted sites stretching not greater than 1000 cm^{-1}. For $\Delta\bar{\nu} > 1000$ cm^{-1}, the linear correlation ceases to exist: this is not strange because we are now comparing strong hydrogen bonds (associated with proton potentials characterized by two minima separated by a low or negligible energy barrier) with medium strength hydrogen bonds in SiOH···B adducts (where the potentials still retain a single minimum). It has been established that, in heterogeneous systems, the ratio of $\Delta\bar{\nu}$ of the strong Brønsted groups (AH) and of $\Delta\bar{\nu}$ of the SiOH groups (used as standard) measured in the same conditions is correlated with the proton affinities by the relation[18,29]

$$PA_{Brønsted} = PA_{SiOH} - A \log (\Delta\bar{\nu}_{Brønsted}/\Delta\bar{\nu}_{SiOH})$$

where

$$PA_{SiOH} = 1390 \text{ kJ mol}^{-1} \quad \text{and} \quad A = 442.5 \text{ kJ mol}^{-1}$$

It is evident that this equation affords a means for measuring the proton affinity of the Brønsted sites of any zeolite. The most important conclusion which can be derived is that $\Delta\bar{\nu}_{Brønsted}/\Delta\bar{\nu}_{SiOH}$ ratio is independent of the base B used to probe the zeolite. The other important conclusion derived from Figure 3 is that the shifts $\Delta\bar{\nu}$ of H−β in the 0−1000 cm^{-1} interval are practically identical to those observed on H−MORD and on H−ZSM-5: this means that the slope of the straight lines corresponding to these zeolites is identical and hence that the acidic character of the Brønsted sites of all of these zeolites is (within the experimental error) nearly equal (and slightly greater than that of H−Y) as far as H−ZSM-5 and H−MORD.

3.5. Case Studies: N_2, CO, H_2O, and THF. In this paragraph the spectroscopic modifications induced by interaction of increasing doses of N_2, CO, H_2O, and THF will be described in detail also with the scope of better elucidating the experimental procedure. Experiments of comparable accuracy have been performed also with C_2H_2, C_2H_4, C_3H_6, CH_3CN, CH_3OH, CH_3CH_2OH, $(CH_3)_2O$, and $(CH_3CH_2)_2O$: however, they will not be described in detail for the sake of brevity.

3.5.1. N_2 and CO. (i) ν(OH) Stretching Region. The effect of the interaction of N_2 and CO at about 100 ± 10 K on the ν(OH) stretching of silanols and of strong Brønsted acid groups is shown in Figure 4a,b and 5a,b, while in Figures 4c and 5c the corresponding spectra in the ν(N−N) and ν(C−O) stretching region is represented. The spectra reported in Figures 4a and 5a correspond to equilibrium pressures of N_2 and CO smaller or equal to those required to complete the formation of 1:1 adducts with the strong Brønsted sites ($p_{CO} \leq 100$ Pa, $p_{N_2} \leq 133$ Pa), while in Figures 4b and 5b the spectra corresponding to the subsequent formation of 1:1 adducts with silanols at higher pressures is shown ($(p_{CO})_{max} = 8$ kPa; $(p_{N_2})_{max} = 12$ kPa).

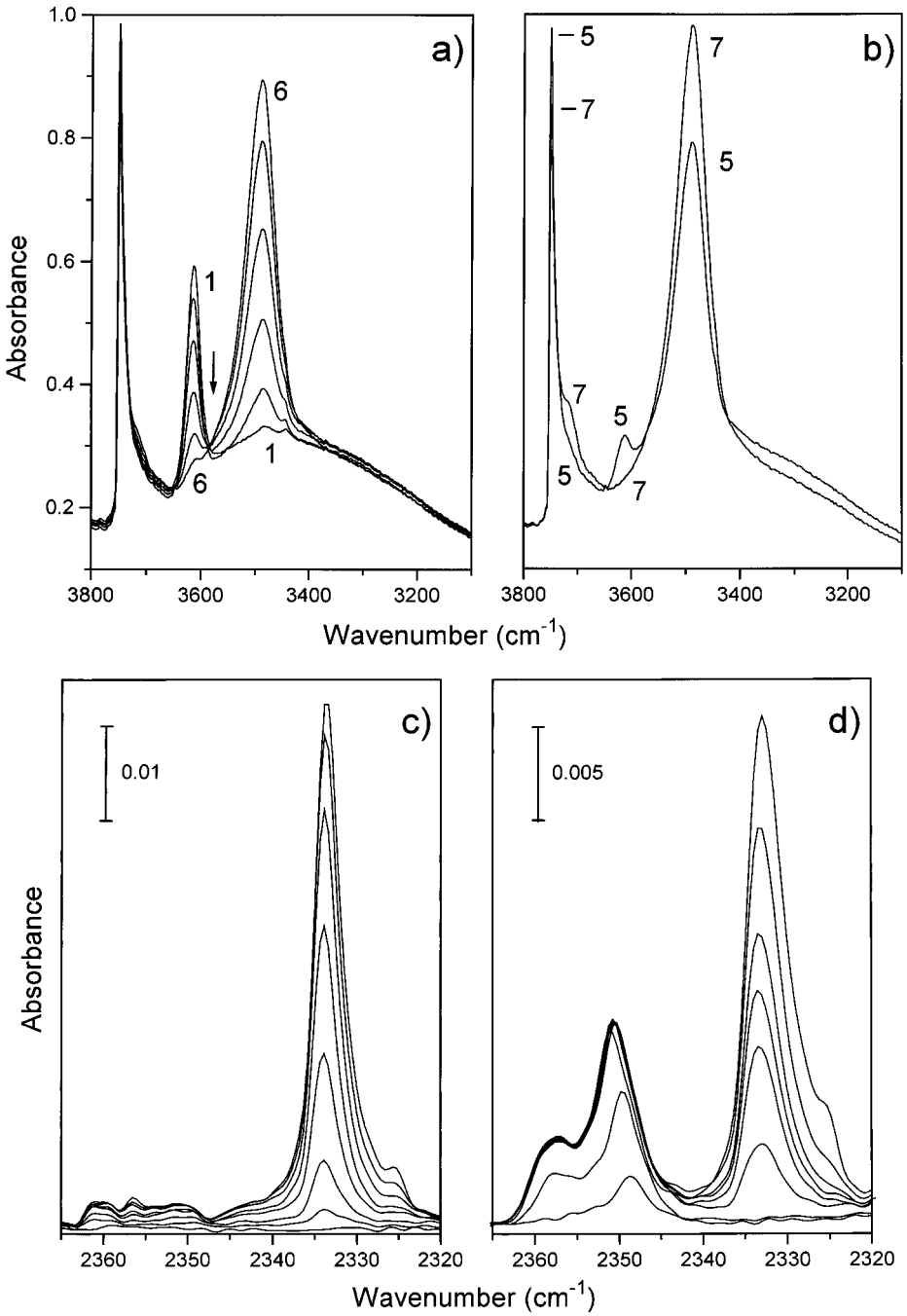

Figure 4. (a) IR spectra of increasing doses of N_2 on H−β outgassed at 673 K. Spectrum 6 corresponds to p = 133 Pa. The presence of an isosbestic point (indicated with the arrow) is unambiguous proof that the 1:1 N_2−Brønsted site interaction is occurring. Spectrum 6, corresponding to full consumption of Brønsted sites, indicates that the 1:1 stoichiometry has been reached. (b) IR spectra of further doses of N_2, corresponding to the initial formation of SiOH···N_2 complexes (the pressure corresponding to the last spectrum is 12 kPa). (c) Evolution of ν(N−N) bands in the 0−12 kPa range. (d) IR spectra of increasing doses of N_2 on a partially dealluminated H−β sample (the most intense spectrum corresponds to p = 12 kPa).

The first comment about the spectra of Figures 4 and 5 is that a direct proportionality exists between the decrease of the intensity of the strong Brønsted site peak (band at 3614 cm^{-1}) and the increase of intensity of the ν(OH···B) band of the 1:1 adduct (B = N_2, 3488 cm^{-1}; B = CO, 3295 cm^{-1}). A clear isosbestic point is observed at 3588 cm^{-1} for N_2 (Figure 4a, arrow in the figure), while in the case of CO (Figure 5a) the isosbestic point is observed at 3501 cm^{-1}. These two facts, together with the quantitative determinations described earlier, confirm that the interaction of strong Brønsted sites with N_2 and CO is a 1:1 process. The ν(OH···B) bands in the OH···N_2 and OH···CO adducts are complex and asymmetric on the higher frequency side; this is due to a certain heterogeneity of the sites.[31] CO does not only perturb the OH groups of the strong Brønsted sites absorbing at 3614 cm^{-1} but also interacts with OH groups absorbing at lower frequencies, as demonstrated by the erosion of the absorption in the 3500−3600 cm^{-1} range. Since the only band which is rising is still at ≅3300 cm^{-1}, we conclude that the broad 3300−3600 cm^{-1} absorption is prevalently associated with Brønsted acid groups in defective sites (nests included). The frequency of these groups is downward shifted with respect to "normal" species, because of weak hydrogen bond interactions with the other groups. As for Figures 4b and 5b, we only remark that the fraction of silanols involved in the interaction is very small for N_2 (only 17% of

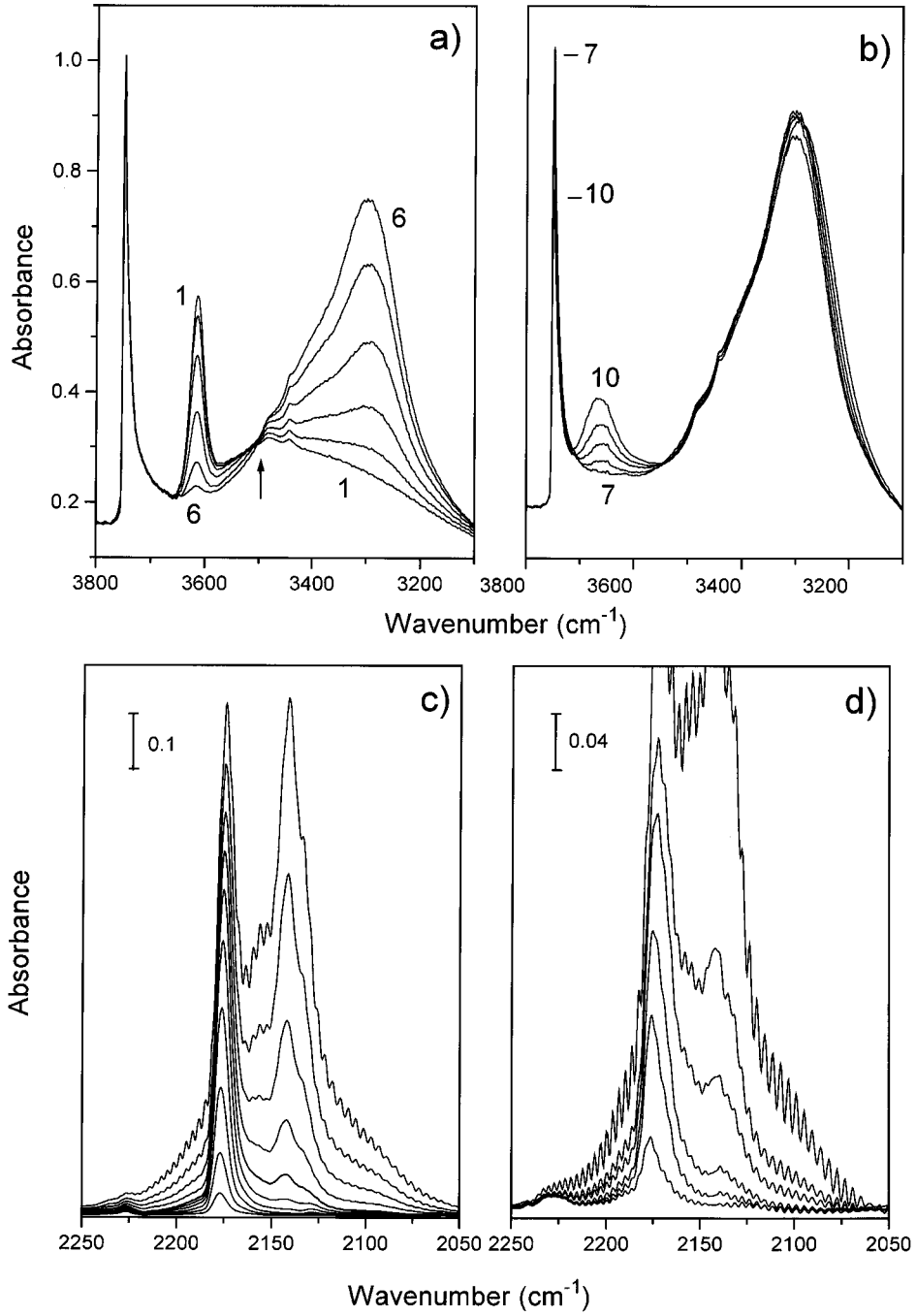

Figure 5. (a) IR spectra of increasing doses of CO on H−β outgassed at 673 K. Spectrum 6 corresponds to $p = 100$ Pa. Also in this case the presence of an isosbestic point is clearly visible (arrow). (b) IR spectra of further doses of CO, corresponding to the formation of SiOH···CO complexes. Spectrum 10 corresponds to $p = 8$ kPa. (c) Evolution of ν(C−O) bands in the 0−8 kPa range. (d) IR spectra of increasing doses of CO on a partially dealluminated H−β sample (the most intense spectrum corresponds to $p = 8$ kPa).

silanols interacts at the maximum investigated pressure of 12 KPa) and is larger for CO (30% for $p_{CO} = 8$ KPa).

(ii) ν(N−N) and ν(C−O) Spectral Range. The N−N stretching modes of the 1:1 adducts between N_2 and the strong Brønsted sites and silanols are observed at 2334 and 2325 cm^{-1} (Figures 4c and 5c), respectively. These frequencies fully agree with those obtained on H−ZSM-5[60] and H−MORD.[35] The data reported in Figure 4c also show that, in our samples, extraframework aluminum is present only in very small proportion, because we observe only a marginal formation of bands in the 2345−2360 cm^{-1} region which are usually attributed to $Al^{3+}_{cus}\cdots N_2$ adducts. A distinctly higher concentration of $Al^{3+}_{cus}\cdots N_2$ adducts is, on the contrary, present on samples outgassed in vacuo at 773 K (Figure 4d) because, as observed on H−ZSM-5 and H−MORD, this thermal treatment is associated not only with water elimination from Brønsted sites but also with migration of Al in extraframework positions.

The ν(CO) mode of the 1:1 adducts is at 2177 cm^{-1} (a frequency very similar to that observed in H−ZSM-5[31] and H−MORD[32]). The ν(CO) band of the adducts with silanols is of more difficult observation because of the presence of the rotovibrational envelope of CO in the gas phase, and it is estimated at 2156 cm^{-1}, i.e., a frequency similar to that found for CO interacting with the silanols of silicalite.[61] At the highest pressures, the abundant formation of CO (liquid-like) physisorbed in the channels is documented by the formation of the intense and complex absorption at 2138 cm^{-1}.[61] Finally, the weak band at 2230 cm^{-1} is due to $Al^{3+}_{cus}\cdots CO$ adducts formed by interaction of CO with highly coordinatively unsaturated aluminum in extraframework positions.[62] As observed for N_2

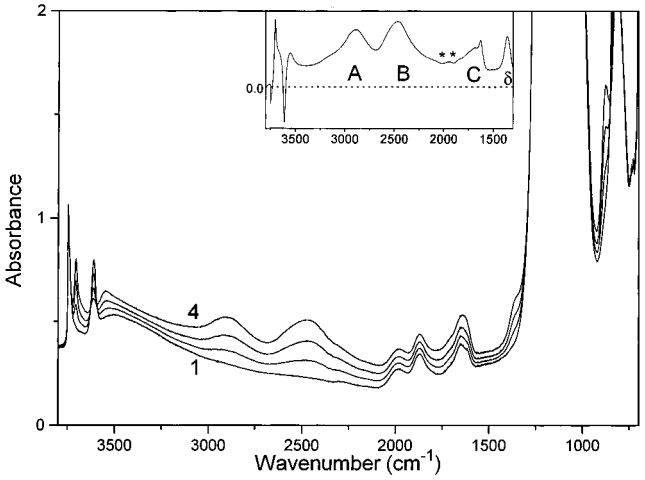

Figure 6. IR spectra of increasing doses of H_2O adsorbed on H−β (H_2O/strong Brønsted sites ratios < 1, curves 1−4). Spectrum 4 corresponds to 85% elimination of the original Brønsted sites. In the inset the background subtracted spectrum corresponding to curve 4 is illustrated. Asterisks as in Figure 2.

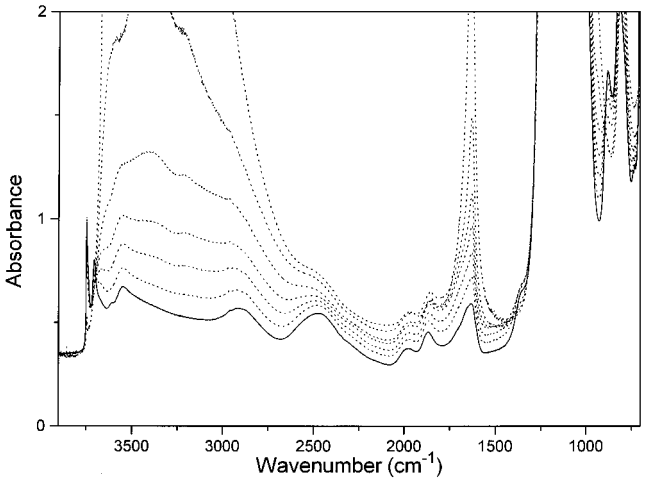

Figure 7. IR spectra of increasing doses of H_2O adsorbed on H−β. Full line spectrum corresponds to a H_2O/strong Brønsted sites ratio ≅ 1 (as also demonstrated by in situ volumetric determination and by parallel gravimetric measurements). The dotted lines correspond to H_2O/strong Brønsted sites ratios > 1.

the decrement of the OH···CO species (associated with the elimination of the strong Brønsted sites induced by the thermal treatment at 773 K) is accompanied by a parallel increment of Lewis acid/CO adducts absorbing at 2230 cm^{-1} (Figure 5c). The effect is less dramatic than that observed with N_2: this is not unexpected since N_2 is a more sensitive probe of strong Lewis acidity than CO. This fact is fully discussed in refs 60 and 63, and it is due to the fact that the strong polarizing fields associated with extralattice Al^{3+}_{cus} are more greatly affecting the intensity of the ν(N−N) than that of the ν(CO) stretching modes.

3.5.2. H_2O. The spectra of the H_2O/H−β system are shown in Figure 6 and Figure 7. The spectra shown in Figure 6 refer to doses of H_2O corresponding to H_2O/sites ratios smaller than 1, while in Figure 7 spectra corresponding to ratios ≥ 1 are reported.

The first series of spectra is documenting the formation of the neutral molecular complex shown in Chart 1, like that found on H−ZSM-5 and H−MORD.[29] With respect to the previous cases, the spectra in Figure 6 are especially interesting because most of the vibrational modes of the complex appear with unprecedented definition. In particular are the following:

CHART 1

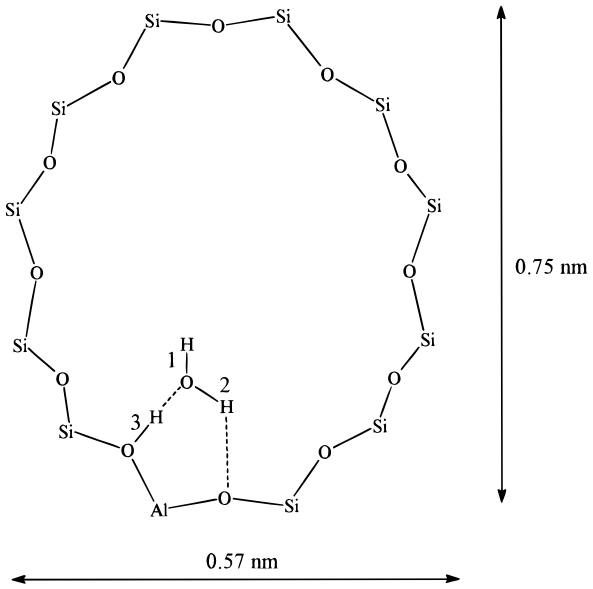

(a) The ν(OH) of group 1 originates the well-defined narrow band at 3710 cm^{-1} (FWHM ≅ 15 cm^{-1}); the frequency and the small width of this band are clear indication that this group is very little interacting either with the opposite wall of the channels (in agreement with the larger radius of the β channels) or with other adjacent molecules. This behavior greatly differentiates β zeolite from H−MORD, and it is more similar to that observed on H−ZSM-5.

(b) The ν(OH···O) mode of group 2 originates a peak at 3525 cm^{-1}, shifted with respect to the mode of group 1 by −185 cm^{-1}; the width is correspondingly greater (FWHM ≅ 60 cm^{-1}). Both observations indicate that the $(OH\cdots O)_{(2)}$ hydrogen bond is very weak.

(c) The $\nu(OH\cdots O)_{(3)}$ mode originates an AB diad of equivalent intensity (see the inset of Figure 6), caused by the Fermi resonance with the $2\delta(OH\cdots O)_{(3)}$ mode. The center of the diad is at 2700 cm^{-1}, i.e. shifted by about −914 cm^{-1} with respect to the frequency of the unperturbed groups. This fact indicates that the strength of the $(OH\cdots O)_{(3)}$ hydrogen bond is medium strong.

(d) In the 1600−1800 cm^{-1} region a complex absorption due to the superposition of a weak C band (see the inset of Figure 6) and of the $\delta(OH_2)$ mode of water is observed (see ref 29 for more details).

(e) The $\delta(OH\cdots O)_{(3)}$ and the $\gamma(OH\cdots O)_{(3)}$ modes are clearly observed at 1360 and 876 cm^{-1}, respectively.

From the above observations it is clear that the spectroscopic properties of the neutral hydrogen bonded species are completely defined. These properties are very similar to those found for the same species on H−ZSM-5 and H−MORD[29,64−70] and to the calculated ones.[69−76]

For H_2O/strong Brønsted site ratios > 1 (Figure 7), the spectrum of the neutral 1:1 complex is gradually eroded because of formation of adsorbed $(H_2O)_n$ clusters interacting with the Brønsted groups. As found on H−ZSM-5 and H−MORD, the clustering already starts before the complete consumption of the Brønsted sites. The erosion is particularly evident for the $\nu(OH)_{(1)}$ band, for the AB doublet, and for δ and γ modes of the $(OH\cdots O)_{(3)}$ group. The observed phenomenon is very similar to that reported for H−ZSM-5 and H−MORD, and the reader is referred to ref 29 for a more detailed discussion. For the time being, we only mention that for ratios > 1 proton transfer is occurring in these zeolites and that the formed clusters

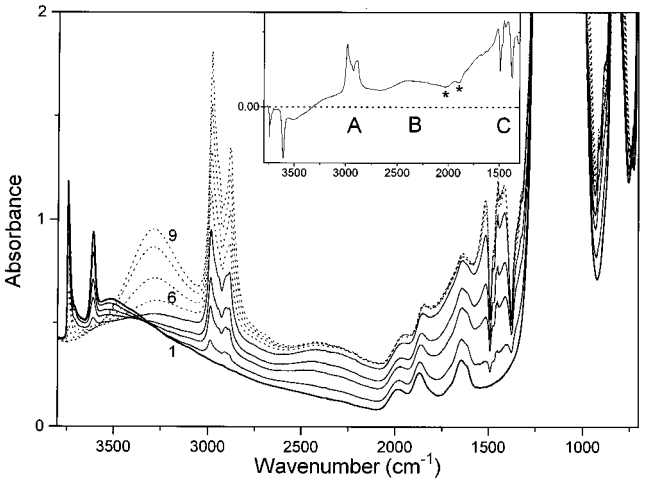

Figure 8. IR spectra of increasing doses of THF adsorbed on H−β. Full line spectra (curves 1−5) correspond to a THF/strong Brønsted sites ratio comprised in the 0−1 interval; the dotted line spectra (curves 6−9) correspond to a THF/strong Brønsted sites ratio > 1. The predominant presence of 1:1 adducts in spectrum 5 is confirmed by simultaneous in situ volumetric determination of the adsorbed quantity and by parallel microgravimetric experiments. In the inset, the background subtracted spectrum corresponding to curve 4 is illustrated. Asterisks as in Figure 2.

CHART 2

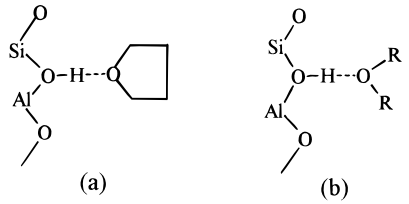

(a) (b)

can be better depicted as $^{+}H(H_2O)_n$. We think that this interpretation holds also in the present case.

3.5.3. THF. The spectra of increasing doses of THF are shown in Figure 8; these spectra are very similar to those of dimethyl and diethyl ethers. Consequently, the conclusions that we are going to derive for THF are also valid for the two others. The full line spectra correspond to THF/strong Brønsted sites ratios < 1 and are associated with progressive formation of the 1:1 complex a (Chart 2), while the dotted line spectra correspond to a ratio ≥ 1. During this second stage THF interacts also with the silanols. A separation of the adsorption process in two stages is somewhat arbitrary, because the interaction with the silanols begins already before the total consumption of the strong Brønsted sites. The formation of OH···B 1:1 adducts originates an ABC structure with $I_C \gg I_B > I_A$. The triad structure is well-shown in the inset of Figure 8. As already observed for the THF/H−MORD and THF/H−ZSM-5 systems,[29] the strong C band is modulated by several deep Evans windows at 1493, 1472, 1440, 1375 cm^{-1}, associated with spectacular and characteristic direct Fermi resonances between the δ modes of the (CH_2) groups and the C band.[30] The corresponding ν(CH_2) stretching bands are at 2987 and 2908 cm^{-1}. It is not excluded that some windows can also be explained by a direct Fermi resonance interaction between the δ(OH) mode of the hydrogen-bonded strong Brønsted sites and the C band. The structure of the triad ($I_C \gg I_B > I_A$) is typical of a very strong hydrogen bond, with a proton potential function characterized by two minima separated by a low-energy gap, or even with a single flat minimum.[39] In the 800−1000 cm^{-1} range we observe two bands at 890 and 916 cm^{-1}: these peaks, however, are not associated with the γ(OH) mode but rather with internal modes of THF.[30]

CHART 3

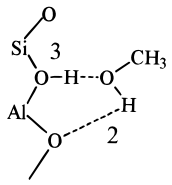

It is interesting to note that, already in the first stage of the absorption, THF interacts with the Brønsted sites responsible for the broad band at 3300−3600 cm^{-1}. This observation gives strength to the hypothesis that at least part of these species has a distinct strength Brønsted acid character. At higher pressures (dotted curves) a progressive erosion of the peak of the external silanols is also observed, due to the formation of the 1:1 adducts with this second class of weaker Brønsted acids; the corresponding ν(OH···B) bond is at 3290 cm^{-1} (FWHM = 250 cm^{-1}). The ν(CH_2) modes of these adducts are observed at slightly lower frequencies (2942, 2882 cm^{-1}) with respect to those of the strongly hydrogen-bonded species.

The sequence of spectra obtained with THF is very similar to those (not shown in detail for brevity) obtained with ethers, and the basic assignment of the bands directly involving the hydrogen bonds in 1:1 adducts (Chart 2b) is consequently the same. It is worth noting that the situation observed for CH_3-OH (Figure 2) is intermediate between that observed for H_2O and ethers and is nearly identical to that observed on H−ZSM-5 and H−MORD.[30] Consequently a similar assignment in terms of the hydrogen-bonded structure illustrated in Chart 3 is very plausible. This neutral structure is characterized by a strong hydrogen bond $(OH\cdots O)_{(3)}$ and by a medium-weaker one $(OH\cdots O)_{(2)}$.

As observed for H_2O, for B/strong Brønsted sites ratios > 1 (B = CH_3OH), the spectrum of the neutral form is gradually eroded, because of the formation of protonated clusters. Also in this case the reader is referred to ref 30 for a more detailed assignment.

3.5.4. Acidity of the External OH Group of Water in Neutral 1:1 Complexes (As Probed by N_2 and CO). The extremely well-defined spectrum of 1:1 water complexes in zeolite H−β (Chart 1) has suggested a further experiment designed to answer the following questions: (i) is it possible to selectively absorb the weak Lewis bases N_2 and CO on the external $(OH)_{(1)}$ of the complex illustrated in Chart 1, with formation of a new H_2O−CO (or N_2) complex (Chart 4), and to estimate (from the induced shift of the $\nu(OH)_{(1)}$ stretching) the acidity of the external OH? (ii) Is it possible to evaluate the indirect effects caused by formation of a hydrogen bond at the external group on the $(OH\cdots O)_{(2)}$ and $(OH\cdots O)_{(3)}$ hydrogen bonds and, hence, to explore the cooperativity effects?

As the answers require an ad hoc designed adsorption experiment at low temperature (≅100 K), a further (and associated) question to answer is: which is the effect of lowering the temperature on the spectrum of the 1:1 complex of water (i.e. before interaction with N_2 and CO)?

The experimental answer to the second question is shown in Figure 9, where curve 1 is the spectrum of the zeolite H−β without adsorbates at room temperature and curves 2 and 3 are the spectra of H−β containing 1:1 complexes performed at 300 and 100 K, respectively. To ensure that every strong Brønsted site was not interacting with more than one H_2O molecule, the amount of dosed H_2O was less than the stoichiometric dose: therefore, spectra 2 and 3 correspond to a H_2O/strong Brønsted sites average ratio of about 4/5. This dosage has been adopted also in the following experiments. The residual features of the

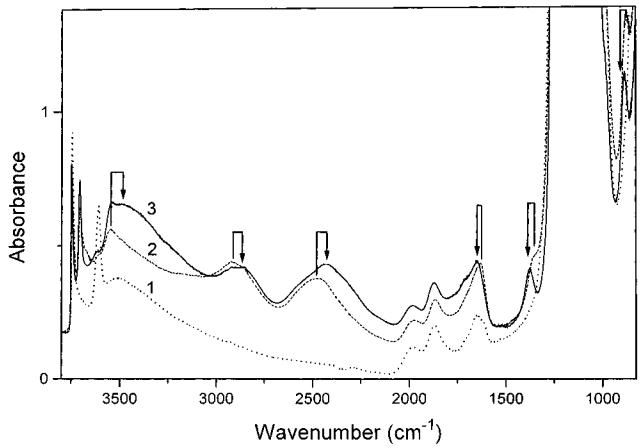

Figure 9. IR spectra of the H−β/H_2O system at 300 and at about 100 ± 10 K. The dotted line (curve 1) represents H−β without adsorbate; the dashed line (curve 2) and the full line (curve 3) are the IR spectra of the H−β/H_2O system at 300 and 100 K, respectively. Arrows indicate the shifts of stretching and bending OH modes.

CHART 4

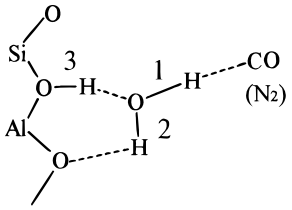

unreacted acid groups appear as a weak band at 3616 cm^{-1}, strongly overlapped with the more intense band at about 3500 cm^{-1}.

Notice how a temperature decrement from 300 to 100 K causes a remarkable variation of intensity and of frequency of the stretching and bending modes of the system (the shifts $\Delta\bar{\nu}$ are evidenced by arrows in Figure 9). In particular are the following:

(i) Stretching Modes. (a) The AB(C) components of the ν-$(OH\cdots O)_{(3)}$ stretching mode (Chart 1) move from 2920 cm^{-1} (A) and 2468 cm^{-1} (B) to 2872 cm^{-1} ($\Delta\bar{\nu}_A = -48$) and to 2422 cm^{-1} ($\Delta\bar{\nu}_B = -46$). Meanwhile the intensity of the A band decreases, while that of the B component increases. The intensity of the C band increases too, originating a large absorption comprised in the 2200 and 1700 cm^{-1} interval.

(b) The frequency of the $\nu(OH\cdots O)_{(2)}$ group (Chart 1) also decreases to 3500 cm^{-1} ($\Delta\bar{\nu} = -47$) with broadening and intensification.

All of these data clearly show that the temperature decrease induces a reinforcement of the strength of the hydrogen bond in both $(OH\cdots O)_{(3)}$ and $(OH\cdots O)_{(2)}$ groups.

(ii) Bending Modes. The δ and γ modes of the $(OH\cdots O)_{(3)}$ groups move upward to 1378 cm^{-1} ($\Delta\bar{\nu} = +18$) and to 886 cm^{-1} ($\Delta\bar{\nu} = +10$), respectively. Both bands become narrower. Once again these data confirm that a reinforcement of the strength of the hydrogen bond is occurring upon lowering the temperature. Also the $\delta(H_2O)$ bending moves upward, but a precise estimation of the shift is not possible because of the presence of the intensified C band. The results previously described are the expected ones for a medium hydrogen bond with double asymmetric minimum. However, measurements at definitely lower temperature should be made in order to derive more definite conclusions on the shape of the potential.

The interaction of CO and N_2 at 100 K with the 1:1 adducts shown in Figure 9 is illustrated in Figures 10 and 11. In these figures, only the difference spectra are reported, because we are interested only in the spectral modifications caused by the weak adsorbates at constant temperature. The main effects of the interaction of N_2 and CO with the H_2O/H−β system can be summarized as follows:

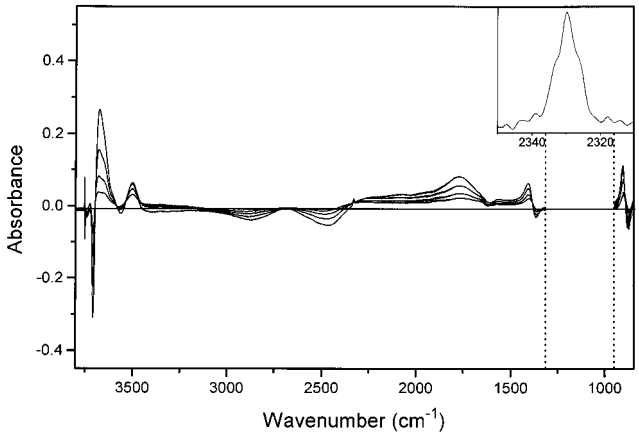

Figure 10. Background subtracted IR spectra of increasing doses of N_2 ($0 < p < 12$ KPa) on the H_2O/H−β system at about 100 ± 10 K (curves 1−5).

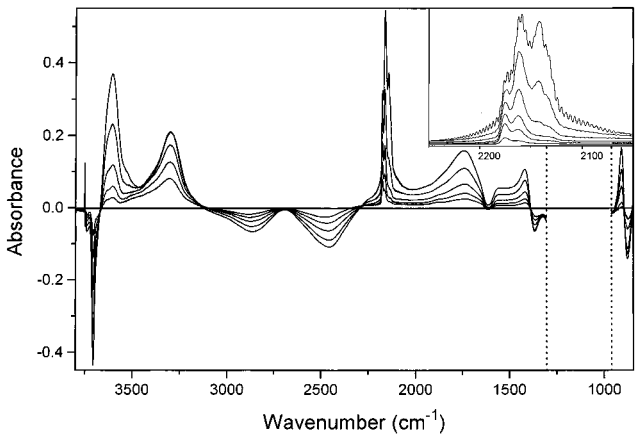

Figure 11. Background subtracted IR spectra of increasing doses of CO ($0 < p < 8$ KPa) on the H_2O/H−β system at about 100 ± 10 K (curves 1−6).

(i) Upon N_2 and CO dosage, the intensity of the stretching mode of the external (OH) group gradually decreases, with formation of a new band at lower frequencies (N_2, $\bar{\nu} = +3678$ cm^{-1}, $\Delta\bar{\nu} = -30$; CO, $\bar{\nu} = +3606$ cm^{-1}, $\Delta\bar{\nu} = -102$); a clear isosbestic point develops at 3696 cm^{-1} for N_2 and at 3668 cm^{-1} for CO. These facts indicate that 1:1 adducts with N_2 and CO (Chart 4) are gradually formed upon increasing the pressure. Since the $\Delta\bar{\nu}$ caused by interaction with N_2 and CO is a measure of the strength of the acid site, an estimation of the acidity of the external proton of adsorbed water can be made. The figures obtained for N_2 and CO are reported in Figure 3. It can be immediately verified that the acid strength of the external groups of adsorbed H_2O is very similar to that of silanols, and much lower than that of the original strong Brønsted site. Owing to the small number of experimental data, it is not possible to verify if a linear relation, characteristic of the external proton of adsorbed water, is holding.

(ii) The bending mode of H_2O is also consumed by interaction with N_2 and CO and presumably shifted to higher frequency: however, after interaction, its position cannot be safely singled out because it is overshadowed by the stronger and broader C band at 1765 (N_2) or 1740 cm^{-1} (CO) (vide infra).

(iii) As far as the manifestations of the $(OH\cdots O)_{(3)}$ group, it is worth noticing that the intensity of the A, B bands decrease,

while the C component at 1765 (N_2) or 1740 cm^{-1} (CO) grows considerably. This phenomenon is due to the further increase of the strength of the $(OH\cdots O)_{(3)}$ bond caused by the charge flow induced by the interaction of the external OH with the N_2 and CO bases (see Figure 1e,f): this is a typical cooperativity effect, and it is associated with an evolution of the proton potential from the shape shown in Figure 1e′ to that of Figure 1f′. Exactly for the same reason (strengthening of the $OH\cdots O_{(3)}$ bond), the δ and γ bending modes move to higher frequencies (1385 (δ) and 889 (γ) cm^{-1} for N_2 and 1403 (δ) and 894 (γ) cm^{-1} for CO). The shift of the δ mode originates a clear isosbestic point at 1381 cm^{-1} for N_2 and at 1386 cm^{-1} for CO.

(iv) The ν(N−N) and ν(C−O) stretching bands of the adducts shown in Chart 4 confirm that the external OH of (neutral) adsorbed H_2O is distinctly less acidic with respect to the original strong Brønsted site of the zeolite. In fact in the inset of Figure 10 three components are observed, at 2326, 2329, and 2333 cm^{-1}, due to the ν(N−N) stretching of N_2 interacting with the strong Brønsted sites, the external OH of H_2O, and the silanols, respectively. From this assignment it is evident that the perturbation induced on the ν(N−N) mode upon formation of the 1:1 adduct shown in Chart 4 is intermediate between that caused by the interaction of N_2 with the strong Brønsted sites and with the silanol (as expected). In a totally similar way, the inset of Figure 11 shows three bands at 2140, 2162, and 2175 cm^{-1}, readily assigned to the stretching mode of CO adsorbed on strong Brønsted sites, external hydrogen of adsorbed water, and silanols. Also in this case the ν(CO) of the 1:1 adduct shown in Chart 4 is intermediate between that of the strong Brønsted sites and of silanols.

4. Conclusions

The acid strength of the strong Brønsted sites of H−β, as probed by measuring the shift $\Delta\bar{\nu}$ induced by the interaction with bases of proton affinity comprised in a wide interval, is found to be nearly identical to that of H−ZSM-5 and H−MORD, but higher than that of H−Y.

Bases with proton affinity < 200 kcal mol^{-1} form hydrogen-bonded 1:1 adducts, characterized by uncompleted proton transfer. Only for bases with PA > 200 kcal mol^{-1} the true proton transfer is really observed with formation of ionic pairs. The basic IR spectroscopy of all of these complexes is discussed in detail and compared with that of the analogous complexes in solution. The structure of mixed H_2O−CO and H_2O−N_2 complexes has also been investigated. The interaction of N_2 and CO with the external OH of H_2O adsorbed on strong Brønsted sites indicates a substantial decrement of acid strength with respect to that of the original strong Brønsted site of the zeolite.

Acknowledgment. This study has been supported by CNR (Progetto Strategico Tecnologie Innovative) and MURST (40%).

References and Notes

(1) Corma, A.; Fornés, V.; Morton, J. B.; Orchilles, A. V. *J. Catal.* **1987**, *107*, 288.
(2) Bellussi, G.; Pazzucconi, G.; Perego, C.; Girotti, G.; Terzoni, G. *J. Catal.* **1995**, *157*, 227.
(3) Matanda, T.; Urata, T.; Kikuchi, E. *Appl. Catal. A* **1995**, *123*, 205.
(4) Smirniotis, P. G.; Ruckenstein, E. *Ind. Eng. Chem. Res.* **1995**, *34*, 1517.
(5) Wang, I.; Chang, Y. *Stud. Surf. Sci. Catal.* **1995**, *92*, 155.
(6) Hutchings, G. J.; Johnston, P.; Lee, D. F.; Warwick, A.; Williams, C. D.; Wilkinson, M. *J. Catal.* **1994**, *147*, 177.
(7) Rao, P. R. H. P.; Massiani, P.; Barthomeuf, D. *Stud. Surf. Sci. Catal.* **1994**, *84*, 1449.
(8) Alvaro, M.; Corma, A.; Garcia, H.; Valencia, S. *Appl. Catal. A* **1995**, *128*, L7.
(9) Camblor, M. A.; Corma, A.; Martin Aranda, R. M.; Perez-Pariente, J. In *Proceedings of the 9th International Zeolite Conference*, Montreal, 1992; Von Ballmoos, R., Higgins, J. B., Treacy, M. M. J., Eds.; Butterworth-Heinemann: Boston, 1993; p 647.
(10) Reddy, K. S. N.; Eapen, M. J.; Joshi, P. N.; Mirajkar, S. P.; Shiralkar, V. P. *J. Inclusion Phenom. Mol. Recognit. Chem.* **1995**, *20*, 197.
(11) Zheng, J.; Dong, J.; Zu, Q.; Liu, Y.; Yan, A. *Appl. Catal. A* **1995**, *126*, 141.
(12) Kladnig, W. F. *J. Phys. Chem.* **1979**, *83*, 765.
(13) Ghosh, A. K.; Curthoys, G. *J. Chem. Soc., Faraday Trans. 1* **1983**, *79*, 147.
(14) Anderson, M. W.; Klinowski, J. *Zeolites* **1986**, *6*, 150.
(15) Parrillo, D. J.; Gorte, R. J. *J. Phys. Chem.* **1993**, *97*, 8786.
(16) Parrillo, D. J.; Gorte, R. J.; Farneth, W. E. *J. Am. Chem. Soc.* **1993**, *115*, 12441.
(17) Pimentel, G. C.; McClellan, A. L. *The Hydrogen Bond*; Pauling, L., Ed.; W. H. Freeman: San Francisco, 1960.
(18) Kubelková, L.; Beran, S.; Lercher, J. A. *Zeolites* **1989**, *9*, 539.
(19) Zecchina, A.; Buzzoni, R.; Bordiga, S.; Geobaldo, F.; Scarano, D.; Ricchiardi, G.; Spoto, G. *Stud. Surf. Sci. Catal.* **1995**, *97*, 213.
(20) Galkin, G. A.; Kiselev, A. V.; Lygin, V. I. *Trans. Faraday Soc.* **1964**, *60*, 256.
(21) Kiselev, A. V. *Surf. Sci.* **1965**, *3*, 292.
(22) Kiricsi, I.; Flego, C.; Pazzucconi, G.; Parker, W. O.; Millini, R.; Perego, C.; Bellussi, G. *J. Phys. Chem.* **1994**, *98*, 4627.
(23) Jia, C.; Massiani, P.; Barthomeuf, D. *J. Chem. Soc., Faraday Trans.* **1993**, *89*, 3659.
(24) Borade, R. B.; Clearfield, A. *J. Phys. Chem.* **1992**, *96*, 6729.
(25) Barzetti, T.; Selli, E.; Moscotti, D.; Forni, L. *J. Chem. Soc., Faraday Trans.* **1996**, *92*, 1401.
(26) Hegde, S. G.; Kumar, R.; Bhat, R. N.; Ratsanamy, P. *Zeolites* **1989**, *9*, 231.
(27) Zecchina, A. To be published.
(28) Wladinger, R. L.; Kerr, G. T.; Ronsinski, E. G. U.S. Patent No. 3308069, 1967.
(29) Zecchina, A.; Geobaldo, F.; Spoto, G.; Bordiga, S.; Ricchiardi, G.; Buzzoni, R.; Petrini, G. *J. Phys. Chem.* **1996**, *100*, 16584.
(30) Zecchina, A.; Bordiga, S.; Spoto, G.; Scarano, D.; Spanò, G.; Geobaldo, F. *J. Chem. Soc., Faraday Trans.* **1996**, *92*, 4863.
(31) Zecchina, A.; Bordiga, S.; Spoto, G.; Scarano, D.; Petrini, G.; Leofanti, G.; Padovan, M. *J. Chem. Soc., Faraday Trans.* **1992**, *88*, 2959.
(32) Bordiga, S.; Lamberti, C.; Geobaldo, F.; Zecchina, A.; Turnes Palomino, G.; Otero Areán, C. *Langmuir* **1995**, *11*, 527.
(33) Buzzoni, R.; Bordiga, S.; Spoto, G.; Scarano, D.; Ricchiardi, G.; Lamberti, C.; Zecchina, A. *Stud. Surf. Sci. Catal.* **1995**, *98*, 104.
(34) Garrone, E.; Chiappetta, R.; Spoto, G.; Ugliengo, P.; Zecchina, A.; Fajula, F. In *Proceedings of the 9th International Zeolite Conference*, Montreal, 1992; Von Ballmoss, R., Higgins, J. B., Treacy, M. M. J., Eds.; Butterworth-Heinemann: Boston, 1993; p 267.
(35) Geobaldo, F.; Lamberti, C.; Ricchiardi, G.; Bordiga, S.; Zecchina, A.; Turnes Palomino, G.; Otero Areán, C. *J. Phys. Chem.* **1995**, *99*, 11167.
(36) Bratos, S. *J. Chem. Phys.* **1975**, *63*, 3499.
(37) Herzberg, G. Molecular Spectra and Molecular Structure, F.R.S.-II. *Infrared and Raman Spectra of Polyatomic Molecules*; Van Nostrand: New York, 1945; p 216.
(38) Odinokov, S. E.; Jogansen, A. V. *Spectrochim. Acta* **1972**, *28A*, 2343.
(39) Böhner, U.; Zundel, G. *J. Phys. Chem.* **1986**, *90*, 964.
(40) Buzzoni, R.; Bordiga, S.; Ricchiardi, G.; Lamberti, C.; Zecchina, A.; Bellussi, G. *Langmuir* **1996**, *4*, 930.
(41) Newsam, J. M.; Tracy, M. M. J.; Koetsier, W. T.; de Gruyter, C. B. *Proc. R. Soc. London* A **1988**, *420*, 375.
(42) Treacy, M. J.; Newsam, J. M. *Nature* **1988**, *332*, 249.
(43) Higgins, J. B.; LaPierre, R. B.; Schlenker, J. L.; Rohrman, A. C.; Wood, J. D.; Kerr, G. T.; Rohrbaugh, W. J. *Zeolites* **1988**, *8*, 446.
(44) Treacy, M. M. J; Newsam, J. M.; Deem, M. W. *Proc. R. Soc. London A* **1991**, *433*, 499.
(45) Tomlinson, S. M.; Jackson, R. A.; Catlow, C. R. A. *J. Chem. Soc., Chem. Commun.* **1990**, 813.
(46) Bourgeat-Lami, E.; Massiani, P.; Di Renzo, F.; Espiau, P.; Fajula, F. *Appl. Catal.* **1991**, *72*, 139.
(47) Papai, I.; Goursot, A.; Fajula, F.; Weber, J. *J. Phys. Chem.* **1994**, *98*, 4654.
(48) Pelmenschikov, A. G.; van Santen, R. A.; Jänchen, J.; Meijer, E. *J. Phys. Chem.* **1993**, *97*, 11071.
(49) Pelmenschikov, A. G.; van Santen, R. A. *J. Phys. Chem.* **1993**, *97*, 10678.
(50) Spoto, G.; Bordiga, S.; Ricchiardi, G.; Scarano, D.; Zecchina, A.; Borello, E. *J. Chem. Soc., Faraday Trans.* **1994**, *90*, 2827.
(51) Geobaldo, F.; Spoto, G.; Bordiga, S.; Lamberti, C.; Zecchina, A. *J. Chem. Soc., Faraday Trans.* **1997**, *93*, 1243.
(52) Bordiga, S.; Ricchiardi, G.; Spoto, G.; Scarano, D.; Carnelli, L.; Zecchina, A.; Otero Areán, C. *J. Chem. Soc., Faraday Trans.* **1993**, *89*, 1843.

(53) Geobaldo, F.; Lamberti, C.; Scarano, D.; Spoto, G.; Zecchina, A. *Proceedings of EUROPACAT-II*, Maastricht, The Netherlands; 1995; p 827.

(54) Knözinger, H. In *The Hydrogen Bond*; Shuster, P., Zundel, G., Sandorfy, C., Eds.; North Holland: Amsterdam, 1976; Vol. III, Chapter 27, p 1263.

(55) Pelmenschikov, A. G.; Morosi, G.; Gamba, A.; Zecchina, A.; Bordiga, S.; Paukshtis, E. A. *J. Phys. Chem*. **1993**, *97*, 11979.

(56) Garrone, E.; Onida, B.; Spanò, G.; Spoto, G.; Ugliengo, P.; Zecchina, A. *Stud. Surf. Sci. Catal*. **1995**, *98*, 99.

(57) Bellamy, L. J.; Hallam, H. E.; Williams, R. L. *Trans. Faraday Soc*. **1958**, *54*, 1120.

(58) Bellamy, L. J.; Pace, R. J. *Spectrochim. Acta* **1969**, *25A*, 319.

(59) (a) Johnson, G. L.; Andrews, L. *J. Phys. Chem*. **1983**, *87*, 1852. (b) Andrews, L.; Davis, S. R. *J. Chem. Phys*. **1985**, *83*, 4983. (c) Andrews, L. *J. Mol. Struct*. **1983**, *100*, 281. (d) Andrews, L. *J. Phys. Chem*. **1984**, *88*, 2940. (e) Andrews, L.; Bahn, R. B.; Arlinghaus, R. T.; Hunt, R. D. *Chem. Phys. Lett*. **1989**, *158*, 564. (f) Andrews, L.; Johnson, G. L. *J. Chem. Phys*. **1983**, *79*, 3670.

(60) Wakabayashi, F.; Kondo, J.; Domen, K.; Hirose, C. *J. Phys. Chem*. **1995**, *99*, 10573.

(61) Zecchina, A.; Bordiga, S.; Spoto, G.; Marchese, L.; Petrini, G.; Leofanti, G.; Padovan, M. *J. Phys. Chem*. **1992**, *96*, 4991.

(62) Jia, C.; Massiani, P.; Barthomeuf, D. *J. Chem. Soc., Faraday Trans*. **1993**, *89*, 3659.

(63) Otero Arean, C.; Turnes Palomino, G.; Geobaldo, F.; Zecchina, A. *J. Phys. Chem*. **1996**, *100*, 6678.

(64) Jentys, A.; Warecka, G.; Derewinski, M.; Lercher, J. A. *J. Phys. Chem*. **1989**, *93*, 4837.

(65) Kubelkovà, L.; Novàkovà, J.; Nedomovà, K. *J. Catal*. **1990**, *124*, 441.

(66) Mirth, G.; Lercher, J.; Auderson, M. W.; Klinowski, J. *J. Chem. Soc., Faraday Trans*. **1990**, *96*, 3039.

(67) Mirth, G.; Kogelbauer, A.; Lercher, J. In *Proceedings of the 9th International Zeolite Conference*, Montreal, 1992; Von Ballmoss, R., Higgins, J. B., Treacy, M. M. J., Eds.; Butterworth-Heinemann: Boston, 1993; p 251.

(68) Wakabayashi, F.; Kondo, J. N.; Domen, K.; Hirose, C. *J. Phys. Chem*. **1996**, *100*, 1442.

(69) Pelmenschikov, A. G.; van Wolput, J. H. M. C.; Jänchen, J.; van Santen, R. A. *J. Phys. Chem*. **1995**, *99*, 3612.

(70) Jobic, H.; Tuel, A.; Krossner, M.; Sauer, J. *J. Phys. Chem*. **1996**, *100*, 19545.

(71) Sauer, J.; Ugliengo, P.; Garrone, E.; Saunders, V. R. *Chem. Rev*. **1994**, *94*, 2095.

(72) Haase, F.; Sauer, J. *J. Phys. Chem*. **1994**, *98*, 3083.

(73) Sauer, J.; Haase, F. *J. Am. Chem. Soc*. **1995**, *117*, 3780.

(74) Sauer, J. *Science* **1996**, *271*, 744.

(75) Krossner, M.; Sauer, J. *J. Phys. Chem*. **1996**, *100*, 6199.

(76) Zygmunt, S. A.; Curtiss, L. A.; Iton, L. E.; Erhardt, M. K. *J. Phys. Chem*. **1996**, *100*, 6663.